aerospace

MDPI

Article

Study on Flow and Heat Transfer Performance of a Rectangular Channel Filled with X-Shaped Truss Array under Operating Conditions of Gas Turbine Blades

Lei Xi, Jianmin Gao, Liang Xu *, Zhen Zhao, Tao Yang and Yunlong Li

State Key Laboratory for Manufacturing Systems Engineering, Xi'an Jiaotong University, Xi'an 710049, China
* Correspondence: xuliang@mail.xjtu.edu.cn; Tel.: +86-186-9186-1949

Abstract: In this investigation, the heat transfer and flow capabilities of an X-shaped truss array cooling channel under various operating conditions of gas turbine blades were thoroughly studied. The influence laws of the inlet Reynolds number, inlet turbulence intensity, wall heat flux and cooling medium (air, steam) on the heat transfer and flow performance of the X-shaped truss array channel were analyzed and summarized. The empirical correlations of friction coefficients and average Nusselt numbers with maximum deviations less than ± 14% were fitted. The results show that the inlet Reynolds number has the most significant effect on the flow and heat transfer performance of the X-shaped truss array channel. When the inlet Reynolds number increases from 20,000 to 200,000, the average Nusselt number of the X-shaped truss array channel is increased by 3.92 times, the friction coefficient is decreased by 12.88%, and the comprehensive thermal coefficient is decreased by 31.19%. Compared with the medium turbulence intensity of Tu = 5%, the average Nusselt number, friction coefficient and comprehensive thermal coefficient of the X-shaped truss array channel at Tu = 20% are increased by 3.70%, 2.51% and 2.79%, respectively. With the increase in the wall heat flux, the friction coefficient of the X-shaped truss array channel roughly shows a trend of first decreasing and then increasing, while the average Nusselt number and the comprehensive thermal coefficient show a trend of first rapidly increasing and then slightly decreasing or remaining unchanged. Compared with air cooling, the average Nusselt numbers of the X-shaped truss array channel of steam cooling are increased by 6.30% to 9.54%, and the corresponding friction coefficients and comprehensive thermal coefficients are decreased by 0.11% to 0.55% and 2.63% to 5.59%, respectively.

Keywords: heat transfer and flow; X-shaped truss array (XTA); rectangular channel; operating conditions; turbine blades

Citation: Xi, L.; Gao, J.; Xu, L.; Zhao, Z.; Yang, T.; Li, Y. Study on Flow and Heat Transfer Performance of a Rectangular Channel Filled with X-Shaped Truss Array under Operating Conditions of Gas Turbine Blades. *Aerospace* **2022**, *9*, 533. https://doi.org/10.3390/aerospace9100533

Academic Editors: Francesco Battista and Marco Pizzarelli

Received: 30 August 2022
Accepted: 19 September 2022
Published: 21 September 2022

1. Introduction

The increase in rotor inlet temperature (RIT) can effectively ameliorate the thermal efficiency and output power of gas turbines [1]. Therefore, the rotor inlet temperature of advanced gas turbines keeps rising (up to 2000 K), making the operating environment of gas turbines more severe [2]. In order to guarantee the reliable and stable operation of gas turbines, it is essential to improve the structural strength as well as the cooling effectiveness of the gas turbine blades.

In recent years, a kind of multifunctional structure, i.e., truss structure, has attracted the attention of researchers in various fields because it has the advantages of remarkable mechanical behaviors such as high specific strength, specific stiffness, toughness and large vibration resistance [3–5], as well as good thermal properties such as high equivalent thermal conductivity and high heat transfer area ratio [6,7]. The popular truss structures are tetrahedron-shaped, pyramid-shaped, octet-shaped, kagome-shaped and body-centered cubic (BBC) truss structures [8]. The main manufacturing techniques for truss

structures include weaving, extrusion, brazing, investment casting and additive manufacturing [9]. Of these, additive manufacturing technology is the most popular manufacturing method for truss structures [10]. Driven by the development of additive manufacturing technology, truss structures with many excellent properties have been gradually applied to the fields of aviation, aerospace, machinery, electronics and energy [11,12]. Joo et al. [13] applied the kagome-shaped truss structure obtained via weaving method to electronic equipment to enhance its heat dissipation capacity. Ullah et al. [14] applied the bio-inspired kagome-shaped truss structure that used additive manufacturing to fabricate an airfoil in order to improve its compressive capacity. Yan et al. [15] applied the X-shaped truss structure manufactured by extrusion technology to the brake disc of an automobile to improve its heat dissipation performance. Akzhigitov et al. [16] applied the kagome-shaped truss structure to a gas turbine rotor blade to strengthen its structural strength. It is expected that if the ribs and pin-fins in the cooling channels are replaced by the truss structures, the structural strength as well as the cooling effect of the gas turbine blades will be tremendously strengthened.

Recently, much work has been devoted to the cooling performance of sandwich panels or rectangular channels filled with various truss structures. Yang et al. [17] numerically studied the heat transfer capacity of sandwich panels filled with kagome-shaped and tetrahedral truss structures. They reported that the sandwich panel with a kagome-shaped truss structure shows better heat transfer capacity than the one with a tetrahedral truss structure. Kemerli et al. [18] investigated the coupled heat transfer properties of a sandwich panel with kagome-shaped truss structure. The results showed that the f (f) and average Nusselt number (Nu_a) of the kagome-shaped truss structure both have a quadratic relationship with the ratio of rod diameter to length. Ma et al. [19] introduced the turbulators of dimple, protrusion and pin-fin in a sandwich panel filled with pyramidal truss structures to enhance the heat transfer properties. Their results showed that this configuration creates a greater pressure drop while enhancing the heat transfer performance of the sandwich panel. Deb et al. [20] investigated the flow and heat transfer properties of various typical truss structures by numerical methods, and accurately predicted the heat transfer coefficients and pressure drops of these truss structures by machine learning approach. Lai et al. [21] studied the heat transfer and flow performance of a heat exchanger with truss array. They declared that the truss rod direction and truss element porosity both exhibits great effect on the fluid flow rate and significantly influences the heat transfer and flow performance of the heat exchanger. Righetti et al. [22] conducted an optimization study on the flow performance of a kind of truss structure with airfoil section. They stated that, under the same heat transfer performance, the pressure reduction of the truss array structure with an airfoil section is reduced by 5% compared to the truss array structure with a round section. Caket et al. [23] reviewed the research status of the heat transfer enhancement effect regarding the 3D truss structures and discovered that the kagome-shaped, tetrahedral, cubic and octet-shaped truss structures are of the greatest interest to researchers. They also pointed out that only 20% of the reported investigations considered the flow performance of the truss structures. Bai et al. [24] conducted an exhaustive investigation on the heat transfer features of a kind of windward bend truss array structure. They suggested that a truss array structure with 2.5 elements in the transverse direction and 6 elements in the longitudinal direction has the highest heat transfer performance. Aider et al. [25] reported that the heat transfer capability and overall thermal performance of the channels filled with truss array structures are, respectively, improved by about 20 times and 3 times when compared with the smooth channels. Shahrzadi et al. [26] numerically studied the heat transfer capability of the BCC truss structure with and without considering the influence of radiation. They stated that the influence of radiation is significant for the heat transfer enhancement effect caused by the body-centered cubic truss structure at a lower Reynolds number (Re). Kaur et al. [27,28] researched the heat transfer and flow performance of various fully periodic truss structures using a numerical approach. They suggested that the

tetrakaidecahedron-shaped truss structure exhibits the highest Nu_a [27], and the octet-shaped truss structure exhibits the largest pressure drop [28].

Currently, various kinds of truss structures have been applied to the mid-chord region and trailing-edge region of gas turbine blades for more efficient cooling and higher mechanical properties. Several studies have been conducted regarding the structural optimization design method [29], mechanical performance analysis [30] and aerodynamic performance analysis [16] of gas turbine blades filled with truss structures. Meanwhile, several investigations have been performed to investigate the flow and heat transfer properties of the cooling channels with different truss structures for the gas turbine blades. Shen et al. [31] utilized the kagome-shaped truss structure to replace the pin-fin in a wedge-shaped channel simplified from the trailing edge of a turbine blade. They reported that the channel with three rows of kagome-shaped truss elements has 6% to 71% greater heat transfer capability compared to the channel with pin-fins at nearly equal pressure drops. Xu et al. [32,33] conducted an optimization study on the heat transfer properties of channels with different truss structures under various aspect ratios to enhance the cooling performance of gas turbine blades. Their results indicated that the heat transfer properties of the optimized channels with various truss structures have been effectively improved. Kaur et al. [34] filled the trailing-edge channel of a gas turbine blade with octet-shaped, tetrakaidecahedron-shaped, face-diagonal-cube-shaped, and cube-shaped truss structures to improve the cooling effect. They reported that the flow performance and comprehensive thermal performance of the cube-shaped truss structure are the best. Liang et al. [35] designed three cooling channels with different truss structures for the trailing-edge cooling of gas turbine blades, and pointed out that the X-shaped, kagome-shaped and BBC truss structures all have better heat transfer and flow performance compared to the pin-fin. Fu et al. [36] studied the influence of kagome-shaped truss structure, BBC truss structure and pin-fin on the performance of film cooling in a gas turbine blade. They stated that these three kinds of cooling structures all can effectually strengthen the film effectiveness of the whole wall, and the enhancement effects of kagome-shaped truss structure and body-centered cubic truss structure are higher than those of pin-fin. Xi et al. carried out the heat transfer and flow analysis [37] and structural parameter optimization [38] of an X-shaped truss array (XTA) channel for gas turbine blades, and then designed three layout schemes for the practical application of the XTA structure in the gas turbine blade mid-chord regions [39].

According to the above literature review, a volume of work has been conducted on the heat transfer and flow properties of different kinds of truss structures, and several studies also have been conducted pertaining to the heat transfer and flow capabilities of channels with truss structures for gas turbine blades. However, the above studies are basically carried out under laboratory conditions, which are quite different from the actual operating conditions of gas turbine blades. Whether the research results mentioned above are applicable to gas turbine blades needs further study. Therefore, it is essential to investigate the heat transfer and flow properties of cooling channels filled with truss structures under the actual operating conditions of gas turbine blades.

In this paper, based on the optimization results in [38] and design results in [39], the heat transfer and flow capabilities of a preferred XTA channel under various operating conditions of the gas turbine high-temperature blades were thoroughly studied. The influence laws of the inlet Re, inlet turbulence intensity (Tu), wall heat flux (q) and cooling medium (air, steam) on the heat transfer and flow performance of the XTA channel were analyzed and summarized. The empirical correlations of f and Nu_a were fitted to increase the practicability of the research results. The results could provide some guidance for the prediction of the cooling performance of advanced high-temperature turbine blades with XTA structures in the future.

2. Research Object

2.1. Physical Model

In order to improve the cooling capacity of the mid-chord area of turbine blades, three layout schemes for a rectangular internal cooling channel filled with XTA were designed in [39]. The three layout schemes are single channel, double subchannels and three subchannels. Because the scheme of three subchannels has better heat transfer performance (63.49% and 18.65% higher than those of single channel and double subchannels [39]) and comprehensive thermal performance (46.49% and 21.96% higher than those of single channel and double subchannels [39]), it was selected as the research object for the numerical simulations in this study. As demonstrated in Figure 1, the XTA cooling channel with three subchannels is a rectangular channel with an aspect ratio of two, which is modeled and simplified from the mid-chord area in a real gas turbine blade [40]. The channel length (L) is 120 mm, the channel height (H) is 20 mm, the channel width (W) is 40 mm and the channel wall thickness (δ) is 1 mm. To reduce the pressure drop and improve the comprehensive thermal performance, the channel was divided into three subchannels along the channel height direction by two thick divider plates with a thickness of 1 mm. Then, the XTA structures were placed in the two near-wall subchannels, and their heights were marked as h. The corresponding subchannel height ratio (h/H) was selected as 0.25 due to its best overall cooling performance (relative to h/H = 0.20; the channel of h/H = 0.25 has the same best comprehensive thermal performance and a better heat transfer performance [39]). Meanwhile, the middle subchannel remained as a smooth channel. The main parameters of the XTA structure are the streamwise spacing ratio (Z_s/C), transverse spacing ratio (X_s/C), truss rod diameter ratio (d/h) and truss rod inclination angle (β), where C is the truss element characteristic length and calculated by the expression of $C = h/\tan(\beta) \times \sin(45°)$. According to the optimum structural parameters obtained at a relatively high Re of 60,000 in [38], the optimal combination of these parameters is as follows: Z_s/C = 1.945, X_s/C = 2.482, d/h = 0.248 and β = 45°. Therefore, 4 rows and 15 columns of truss elements were disposed in the two near-wall subchannels.

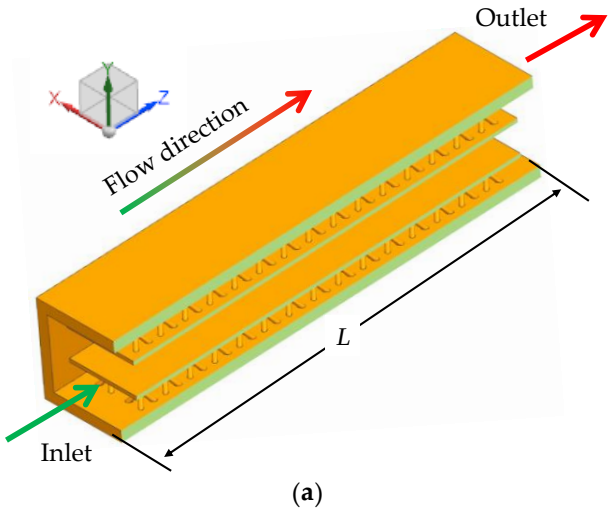

(**a**)

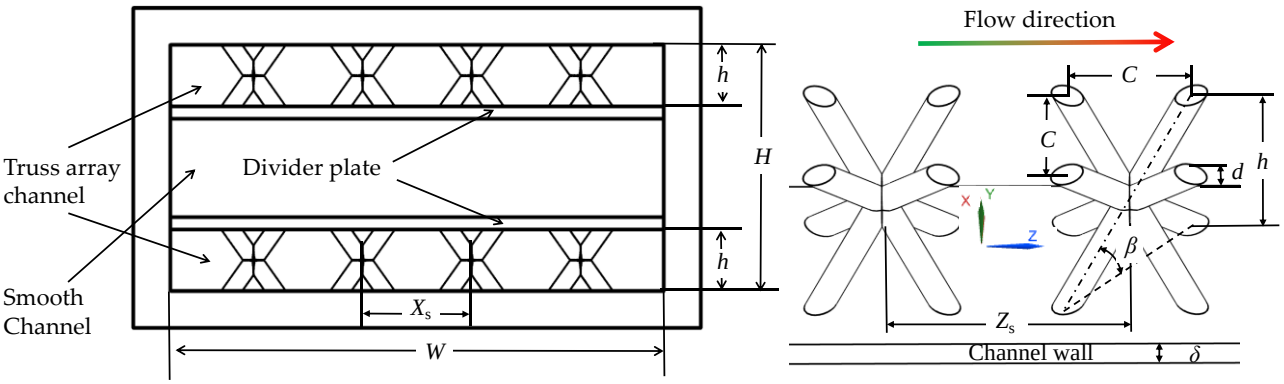

Figure 1. Physical Model: (**a**) sketch map; (**b**) structural drawing.

2.2. Data Reduction

The *Re* is computed by:

$$Re = uD/v \tag{1}$$

where D is the equivalent diameter of the channel, computed by $D = 2WH/(W + H)$; v and u are the kinematic viscosity and inlet cooling medium (air or steam) velocity.

The local Nusselt number (Nu) is defined by:

$$Nu = qD/[(T_w - T_c)\lambda] \tag{2}$$

where q is the local wall heat flux; λ is the heat conductivity of the cooling medium; T_w is the local wall temperature; T_c is the local bulk fluid temperature calculated in CFX-post, as the authors of the present study previously reported in [39].

The friction coefficient (f) is expressed as:

$$f = \Delta pD/(2\rho Lu^2) \tag{3}$$

where Δp is the channel pressure drop; ρ is the cooling medium density.

The comprehensive thermal coefficient (F) is expressed as:

$$F = (Nu_a/Nu_0)/(f/f_0)^{1/3} \tag{4}$$

where Nu_0 and f_0 are the average Nusselt number and friction coefficient of the smooth channel, and are computed by the expressions of $Nu_0 = 0.023Re^{0.8}Pr^{0.4}$ and $f_0 = (1.58\ln Re - 3.28)^{-2}$, respectively.

3. Numerical Simulation Approach

3.1. Numerical Simulation Model

In this investigation, the fluid–solid coupled heat transfer model was built for the XTA channel. As demonstrated in Figure 2a, the fluid–solid coupled heat transfer model mainly comprises the solid domain and fluid domain of the XTA channel, as well as the fluid domains of two extended smooth channels. The length of each smooth channel is 200 mm, so the cooling fluid entering the XTA channels is fully developed. The two adjacent fluid domains are connected by the fluid–fluid interface, and the adjacent solid domain and fluid domain are connected by the fluid–solid interface. It is worth noting that only half of the XTA channel was modeled because of the symmetrical feature of the structure along the mid-section of the channel. Then, each computational domain of the coupled model was separately meshed by Workbench. The fluid domains of smooth channels were divided into structured meshes. The fluid domain and solid domain of the XTA channel were divided into unstructured meshes, as displayed in Figure 2b. The solid domain of the XTA channel entirely consists of tetrahedral meshes. The fluid domain of

the XTA channel consists of the prismatic meshes at the boundary layers and the tetrahedral meshes in the channel main body. The first layer height of the prismatic meshes was set to 0.001 mm. The height ratio and layer number of the prismatic meshes were set to 1.2 and 15. In this way, the values of y^+ near the wall were close to one. The tetrahedral meshes of the truss rods as well as their adjacent regions were refined with a smallest size of 0.03 mm. The largest tetrahedral mesh size was determined by the grid independence test. According to the grid independence test results [39] previously reported by the authors of the present study, the total mesh number of 8.6 million can meet the requirements of the grid independence test, and the corresponding largest mesh size is 1.2 mm. Finally, all meshes were smoothed and matched to elevate the calculation precision of the fluid–solid coupled heat transfer model.

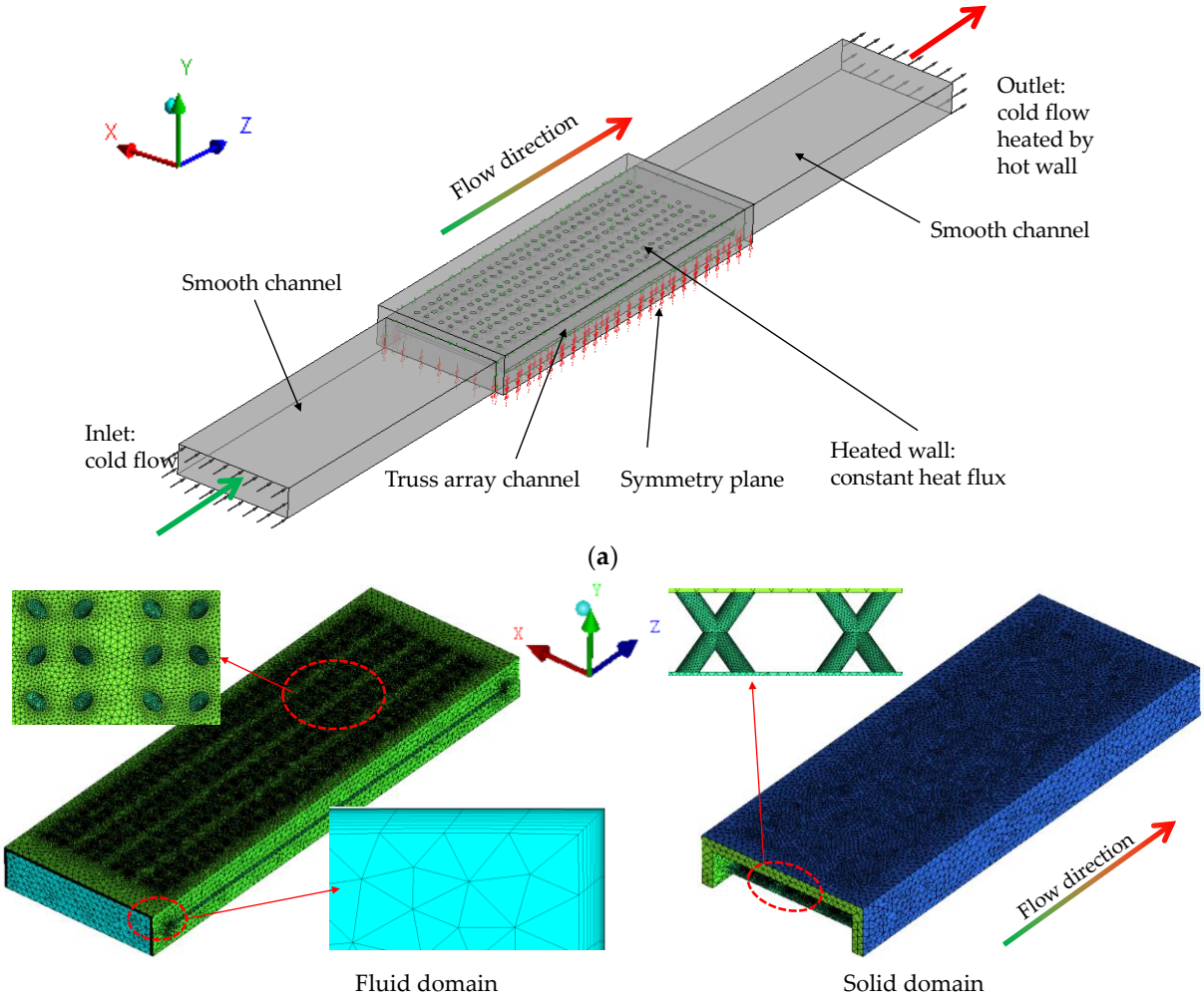

Figure 2. Numerical simulation model: (**a**) calculation model; (**b**) grid model.

3.2. Numerical Calculation Methods

The fluid–solid coupled heat transfer method was adopted to predict the heat transfer and flow capabilities of the XTA channel under the actual operating conditions of the gas turbine high-temperature blades in this work. All the numerical simulations were completed by the CFX-solver. During the numerical simulations, the cooling medium in the XTA channel was assumed to be three-dimensional, steady, compressible, and free of gravity and turbulent fluid. The fully implicit coupled multigrid was utilized to compute the RANS equations. The finite difference approach with the bounded central difference scheme was adopted to discretize the control equations of mass, momentum and energy

[38]. The advection scheme option and the turbulence numerical option were set as the high-resolution scheme. The heat transfer scheme option was assigned as the total-energy scheme. The turbulent transport equations were solved by the turbulence model of SST *k-ω*. This is because the SST *k-ω* has a better prediction effect on the heat transfer capability of the XTA channel, which has been proved by the verification results reported in [37–39]. The heat conduction equation was solved to predict the heat conduction behavior of the channel solid domain. Finally, when the residual levels of the governing equations all converged to 10^{-6}, the numerical simulations were completed.

The main control equations [2] are as follows:

$$\frac{\partial \rho}{\partial t} + \nabla \cdot (\rho \boldsymbol{U}) = 0 \tag{5}$$

$$\frac{\partial (\rho \boldsymbol{U})}{\partial t} + \nabla \cdot (\rho \boldsymbol{U} \otimes \boldsymbol{U}) = -\nabla p + \nabla \cdot \tau + \boldsymbol{S}_M \tag{6}$$

$$\frac{\partial (\rho h_{\mathrm{tot}})}{\partial t} - \frac{\partial p}{\partial t} + \nabla \cdot (\rho \boldsymbol{U} h_{\mathrm{tot}}) = \nabla \cdot (\lambda \nabla T) + \nabla \cdot (\boldsymbol{U} \cdot \tau) + \boldsymbol{U} \cdot \boldsymbol{S}_M + \boldsymbol{S}_E \tag{7}$$

where τ is the stress tensor; h_{tot} is the total enthalpy.

3.3. Boundary Conditions

The actual cooling conditions of gas turbine blades are very harsh. When the cooling air is extracted from the medium pressure stage of the compressor, the air pressure can reach more than 2.5 MPa and the air temperature can reach more than 723 K. According to the actual cooling conditions of gas turbine blades, the numerical boundary conditions for the XTA channel in this work were designed. The channel mid-section was designated as the symmetrical boundary condition because only half of the XTA channel was numerically modeled, as displayed in Figure 2a. The channel inlet was designated as the boundary conditions of static temperature and turbulence intensity as well as uniform normal velocity calculated according to the inlet *Re*, and the channel outlet was designated as the boundary condition of mean static pressure with a fluctuation of 5%. The channel outside walls were designated as the boundary condition of constant heat flux, the surfaces between the solid domain and the fluid domain were designated as the fluid–solid interface and other surfaces were designated as the non-slip and adiabatic boundary conditions. The parameter ranges of the above boundary conditions are as follows: the inlet static temperature is 723 K, the inlet *Re* varies from 20,000 to 200,000, the inlet *Tu* varies from 1% to 20%, the *q* varies from 1 kW·m^{-2} to 100 kW·m^{-2} and the outlet average static pressure is 2.5 MPa. The physical parameters of the cooling medium at the initial static pressure (p_r) of 2.5 MPa and initial static temperature (T_r) of 723 K are as follows: the density, Prandtl number (*Pr*), dynamic viscosity, thermal conductivity and specific heat capacity at constant pressure, at the channel inlet, were 9.259 kg·m^{-3}, 0.697, 0.0000348 Pa·s, 0.054 W·m^{-1}·K^{-1} and 1.087 kJ·kg^{-1}·K^{-1} for the air and were 7.685 kg·m^{-3}, 0.939, 0.0000265 Pa·s, 0.0627 W·m^{-1}·K^{-1} and 2.223 kJ·kg^{-1}·K^{-1} for the steam.

3.4. Numerical Method Verification

The numerical method verification was carried out to ensure the accuracy of the numerical calculation results for the XTA channel in this work. The numerical calculated Nu_a of three widely used turbulence models of (SST *k-ω*, standard *k-ε* and standard *k-ω*) was compared with the experimentally measured Nu_a of the XTA channel (d/h = 0.2, Z_s/C = 2 and X_s/C = 2) reported in [38]. As can be seen in Table 1, among these three turbulence models, the calculated Nu_a of the standard *k-ε* turbulence model is larger than that of the experimentally measured result, while the calculated Nu_a of the standard *k-ω* and SST *k-ω* models is smaller than that of the experimental result. The prediction deviation of the standard *k-ε* model is the lowest when the *Re* is 10,000, and the prediction deviation of the

SST k-ω model is the lowest when the Re varies from 20,000 to 50,000. On the whole, the SST k-ω turbulence model can most accurately predict the Nu_a of the XTA channel, with a largest deviation of −12.71% and a mean deviation of −5.98%. Consequently, the SST k-ω model was selected to accomplish the numerical calculations in this investigation.

Table 1. Validation of numerical methods.

Test Data in [38]		**Numerical Data of Standard k-ε**		**Numerical Data of Standard k-ω**		**Numerical Data of SST k-ω**	
Re	Nu_a	Nu_a	Error/%	Nu_a	Error/%	Nu_a	Error/%
10,000	123.96	131.23	5.86	100.00	−19.33	108.20	−12.71
20,000	165.04	193.22	17.07	149.34	−9.51	156.23	−5.33
30,000	216.64	254.35	17.41	189.35	−12.60	206.14	−4.85
40,000	242.33	282.66	16.64	222.67	−8.11	237.81	−1.87
50,000	270.39	302.65	11.93	243.13	−10.08	256.52	−5.13

4. Results Analysis and Discussion

4.1. Effects of Inlet Reynolds Number

Figure 3 displays the contour maps of Nu on the truss rod surface and channel wall and the plots of velocity vector in the channel for the XTA channel at various inlet Re under the actual operating conditions (p_r = 2.5 MPa, T_r = 723 K) of the gas turbine high-temperature blades. The other operating conditions are as follows: Tu = 5%, q = 25 kW·m^{-2}. Since the distribution characteristics of the Nu and velocity fields of the whole channel have been discussed in detail in [37,39], only the influences of various operating conditions on the heat transfer and flow characteristics of the fully developed section of the XTA channel were analyzed in this investigation. It can be seen from Figure 3a that as the inlet Re varies from 20,000 to 200,000, the Nu on both the truss rod surface and the channel wall are markedly increased. Especially, the heat transfer enhancement effects caused by increasing Re at the regions of the channel wall between two rows of truss elements as well as the truss rod windward surfaces near the truss rod ends are most obvious. This implies that the inlet Re can still very effectually strengthen the heat transfer performance of the XTA channel under the actual operating conditions of the gas turbine high-temperature blades. It can be found from Figure 3b that the increase in the inlet Re obviously raises the flow velocity between two columns of truss elements as well as around the truss rods, and slightly increases the size of the vortexes formed around the truss rods in the XTA channel. Therefore, the increase in inlet Re may increase the pressure drop of the XTA channel.

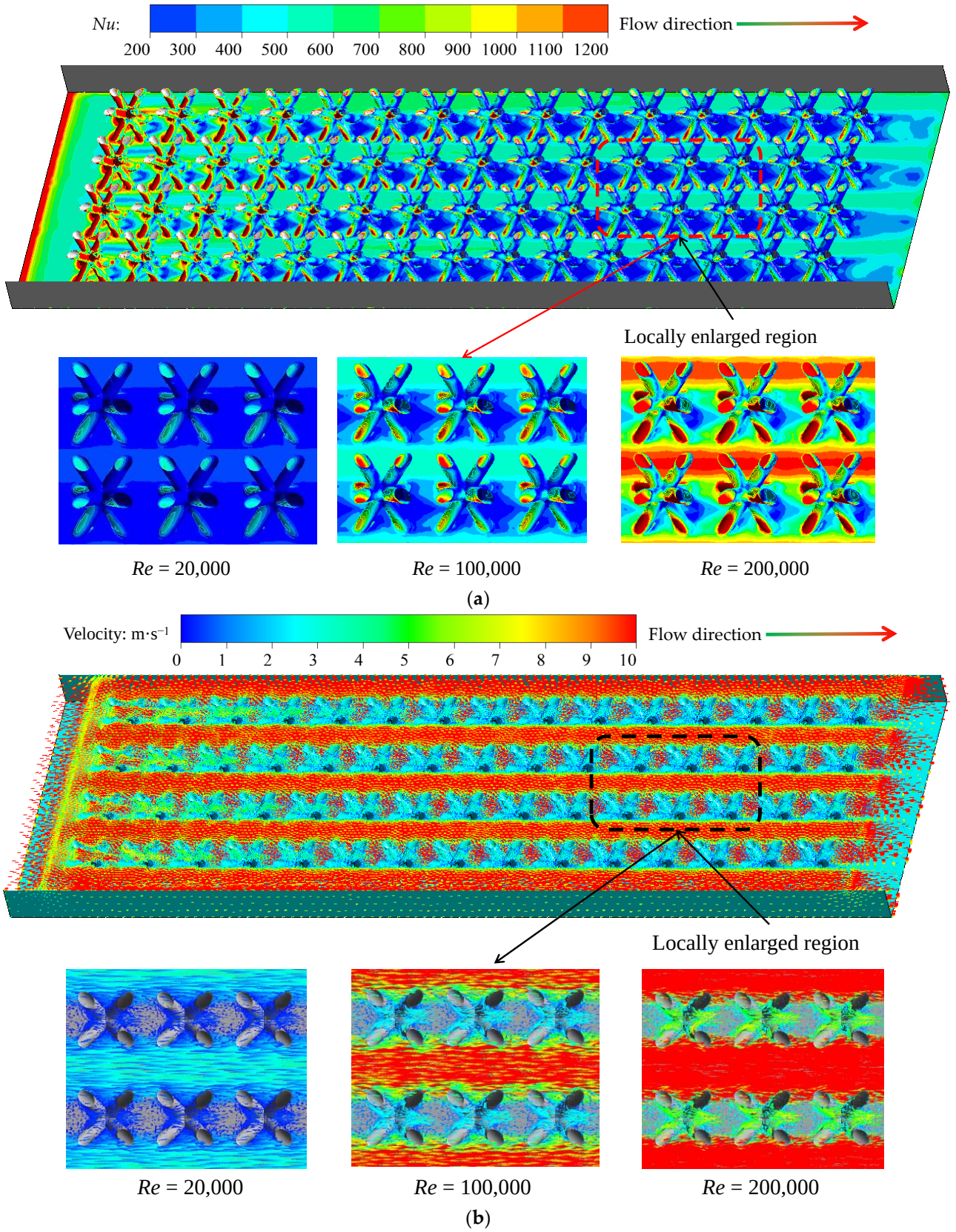

Figure 3. Distributions of heat transfer and flow field at various inlet *Re* under the actual operating conditions of gas turbine blades: (**a**) heat transfer distributions; (**b**) flow field distributions.

Figure 4 shows the variation trends of the Nu_a, f and F of the XTA channel with the inlet *Re* under the actual operating conditions (p_r = 2.5 MPa, T_r = 723 K) of the gas turbine

high-temperature blades. As can be seen from Figure 4, under the actual operating conditions of gas turbine blades, the increase in *Re* makes the Nu_a of the XTA channel gradually increase, makes the *f* of the XTA channel first slowly decrease and then basically remain unchanged, and makes the *F* of the XTA channel gradually decrease. This indicates that the increase in *Re* weakens the heat transfer enhancement effect of the XTA under the condition of equal pump power, which can be inferred from the above results and Equation (5). Compared with the results in [39], it can be found that the influence law of *Re* on the heat transfer performance, flow performance and comprehensive thermal performance of the XTA channel under the actual operating conditions of gas turbine blades is basically the same as that under the laboratory conditions. This indicates that the research results under laboratory conditions reported in [39] can be extended to the actual operating conditions of gas turbine blades. According to the calculation results, under the actual operating conditions of gas turbine blades, when the *Re* increases from 20,000 to 200,000, the Nu_a of the XTA channel is increased by 3.92 times, the *f* is decreased by 12.88%, and the *F* is decreased by 31.19%.

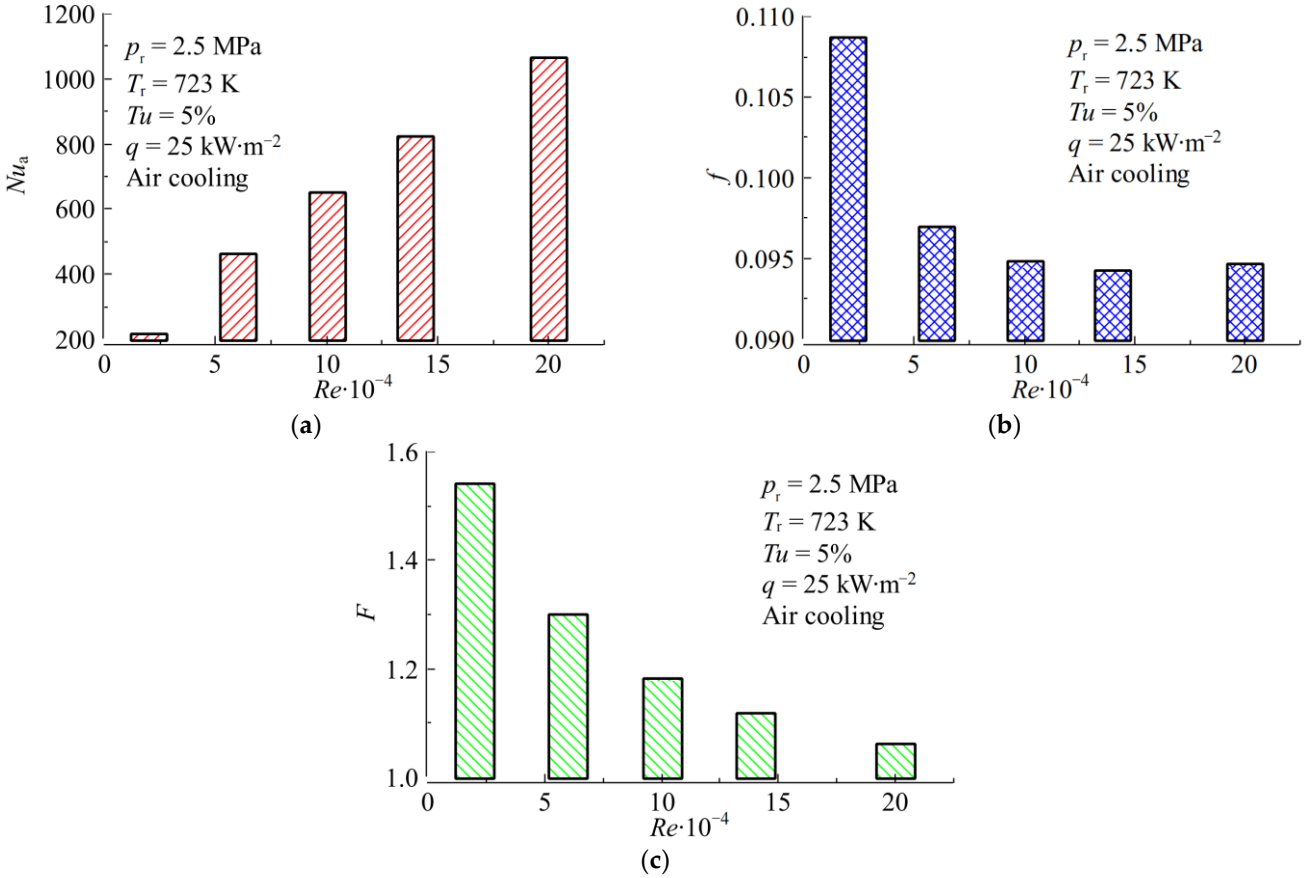

Figure 4. Effects of inlet *Re* on the cooling performance of XTA channel under actual operating conditions of gas turbine blades: (**a**) heat transfer performance; (**b**) flow performance; (**c**) comprehensive thermal performance.

4.2. Effects of Inlet Turbulence Intensity

Figure 5 demonstrates the contour maps of *Nu* on the truss rod surface and channel wall and the plots of velocity vector in the channel for the XTA channel at various inlet *Tu* under the actual operating conditions (p_r = 2.5 MPa, T_r = 723 K) of the gas turbine high-temperature blades. The other operating conditions are as follows: *Re* = 100,000, *q* = 25 kW·m^{-2}. As shown in Figure 5a, when the inlet *Tu* varies from 1% to 10%, the *Nu* on the truss rod surface and the channel wall of the XTA channel are both slightly improved. When the inlet *Tu* varies from 10% to 20%, the increase in *Nu* on both the truss rod surface

and the channel wall is very insignificant. On the whole, under the actual operating conditions of gas turbine blades, the increase in inlet *Tu* can enhance the local heat transfer effect of the XTA channel to a lesser extent. As can be found from Figure 5b, when the inlet *Tu* varies from 1% to 10%, the flow velocity of the cooling fluid in the XTA channel slightly increases. When the inlet *Tu* varies from 10% to 20%, the flow velocity of the cooling fluid in the channel hardly changes. The inlet *Tu* hardly affects the sizes of the vortexes in the channel. On the whole, the increase in inlet *Tu* has little effect on the flow field distribution in the XTA channel under the actual operating conditions of gas turbine blades.

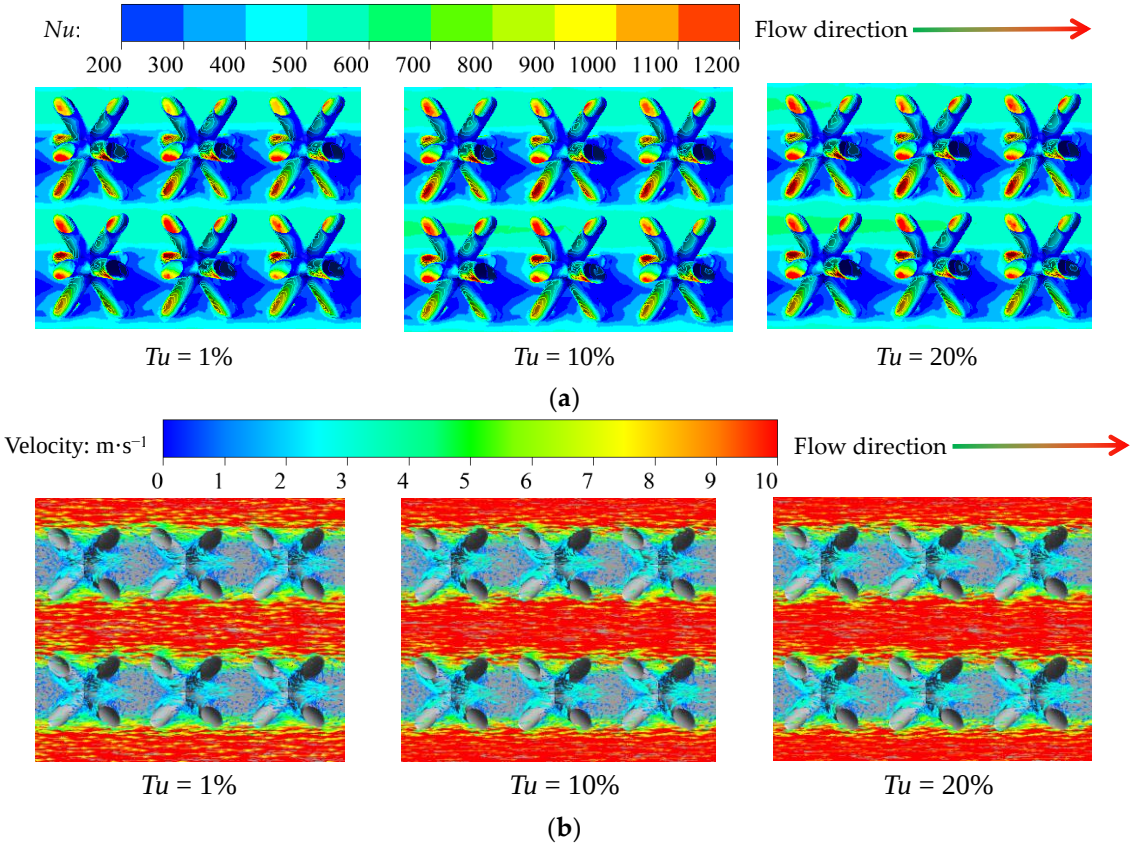

Figure 5. Distributions of heat transfer and flow field at various inlet *Tu* under the actual operating conditions of gas turbine blades: (**a**) heat transfer distributions; (**b**) flow field distributions.

Figure 6 illustrates the influence curves of the inlet *Tu* on the Nu_a, *f* and *F* of the XTA channel under the actual operating conditions (p_r = 2.5 MPa, T_r = 723 K) of gas turbine blades. Generally, *Tu* = 1% is low turbulence intensity, *Tu* = 5% is medium turbulence intensity and *Tu* ≥ 10% is high turbulence intensity. As can be seen from Figure 6a, when the inlet *Tu* varies from 1% to 5%, the Nu_a of the XTA channel changes with a very small increase. When the inlet *Tu* changes from 5% to 10%, the Nu_a of the XTA channel shows a faster increase trend. When the inlet *Tu* is higher than 10%, the increase rate of the Nu_a of the channel becomes slow again. On the whole, the increase in inlet *Tu* increases the Nu_a of the XTA channel. This is because increasing the inlet *Tu* strengthens the heat exchange between the cold fluid and the hot channel wall, thus enhancing the heat transfer performance of the XTA channel. According to the calculation results, under different *Re*, the Nu_a of the XTA channel is decreased by about 0.46% at the lowest inlet turbulence intensity (*Tu* = 1%) and increased by about 3.70% at the highest inlet turbulence intensity (*Tu* = 20%) compared with the medium inlet turbulence intensity (*Tu* = 5%). As shown in Figure 6b, the increase in the inlet *Tu* also increases the *f* of the XTA channel. Specifically, the *f* of the XTA channel slightly changes in the cases of low turbulence intensity (*Tu* = 1%) and medium turbulence intensity (*Tu* = 5%). In the case of high turbulence intensity (*Tu* ≥

10%), the *f* of the XTA channel comparatively rapidly changes. The reason why the *f* of the channel increases with the inlet *Tu* is that the increase in the inlet *Tu* indicates the increase in the pulsation velocity of the cooling fluid, which leads to the more turbulent cooling fluid in the channel, and thus increases the *f* of the channel. At various *Re*, compared with the medium turbulence intensity (*Tu* = 5%), the *f* of the XTA channel is reduced by about 0.10% at the lowest turbulence intensity (*Tu* = 1%) and increased by about 2.51% at the highest turbulence intensity (*Tu* = 20%). As shown in Figure 6c, the increase in inlet *Tu* can slightly improve the comprehensive thermal performance of the XTA channel. When the inlet *Tu* is increased from 1% to 5%, the *F* of the XTA channel is only increased by 0.51%. When the inlet *Tu* is increased from 5% to 20%, the *F* of the XTA channel is improved by about 2.79%. In conclusion, under the actual operating conditions of gas turbine blades, changing the inlet *Tu* of the cooling fluid has little effect on the heat transfer performance, flow performance and comprehensive thermal performance of the XTA channel.

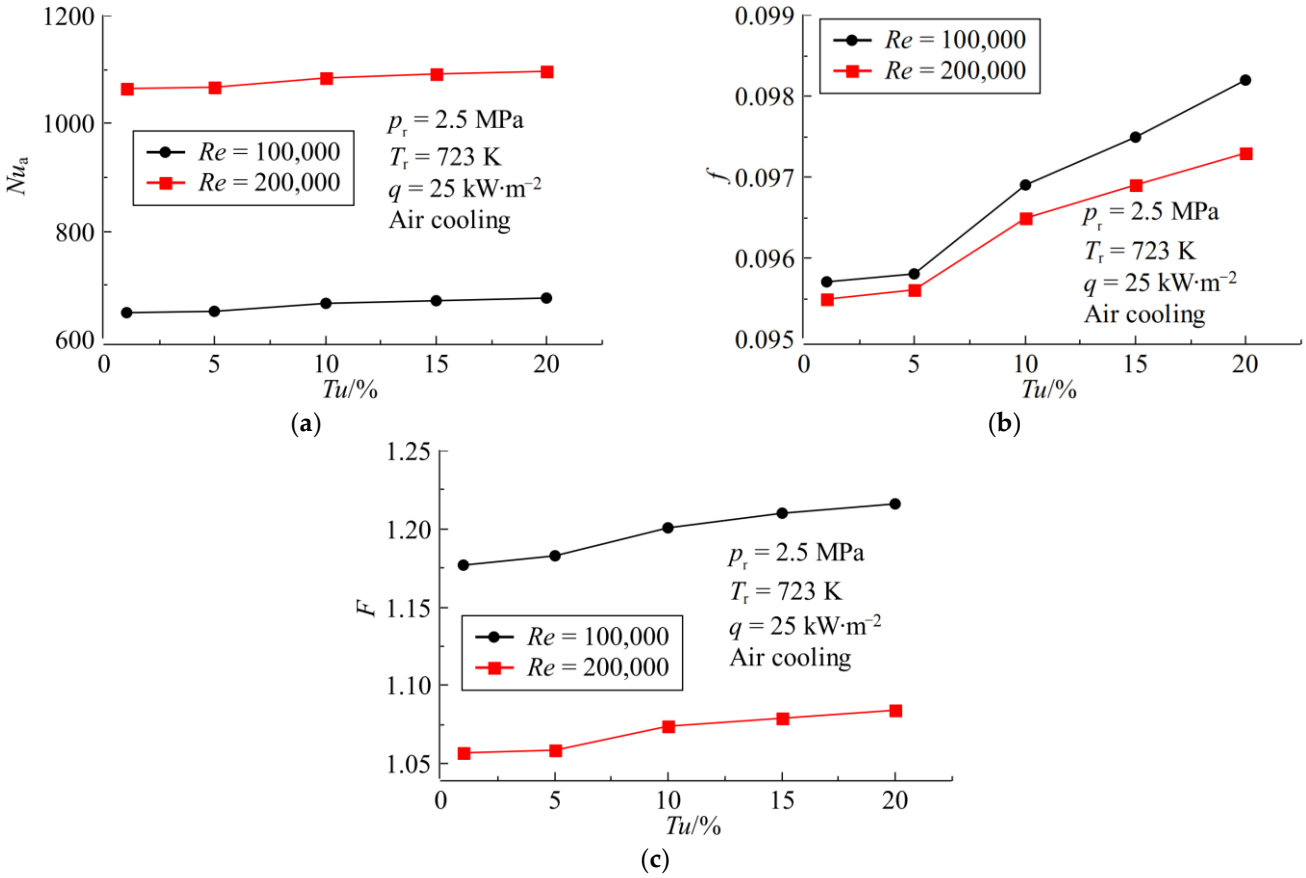

Figure 6. Effects of inlet *Tu* on the cooling performance of XTA channel under actual operating conditions of gas turbine blades: (**a**) heat transfer performance; (**b**) flow performance; (**c**) comprehensive thermal performance.

4.3. Effects of Wall Heat Flux

Figure 7 shows the contour maps of *Nu* on the truss rod surface and channel wall and the plots of velocity vector in the channel for the XTA channel at various *q* under the actual operating conditions (p_r = 2.5 MPa, T_r = 723 K) of the gas turbine high-temperature blades. Other operating conditions are as follows: *Re* = 100,000, *Tu* = 5%. As shown in Figure 7a, for the channel wall of the XTA channel at *Re* = 100,000, the *Nu* nearly remain unchanged along with the increase in the *q*. For the truss rod surfaces of the XTA channel at *Re* = 100,000, only the *Nu* on the truss rod windward surfaces near the truss rod ends are enhanced to some extent when the *q* varies from 1 kW·m^{-2} to 50 kW·m^{-2}, and the *Nu* on

other regions at various q are almost unchanged. All in all, the influence of q on the heat transfer performance of the XTA channel is not significant at Re = 100,000 under the actual operating conditions of gas turbine blades. As shown in Figure 7b, the q hardly influences the flow velocity of the cooling fluid or the sizes of the vortexes in the XTA channel at Re = 100,000. This indicates that changes in the q have little influence on the flow performance of the cooling air in the XTA channel under the actual operating conditions of gas turbine blades.

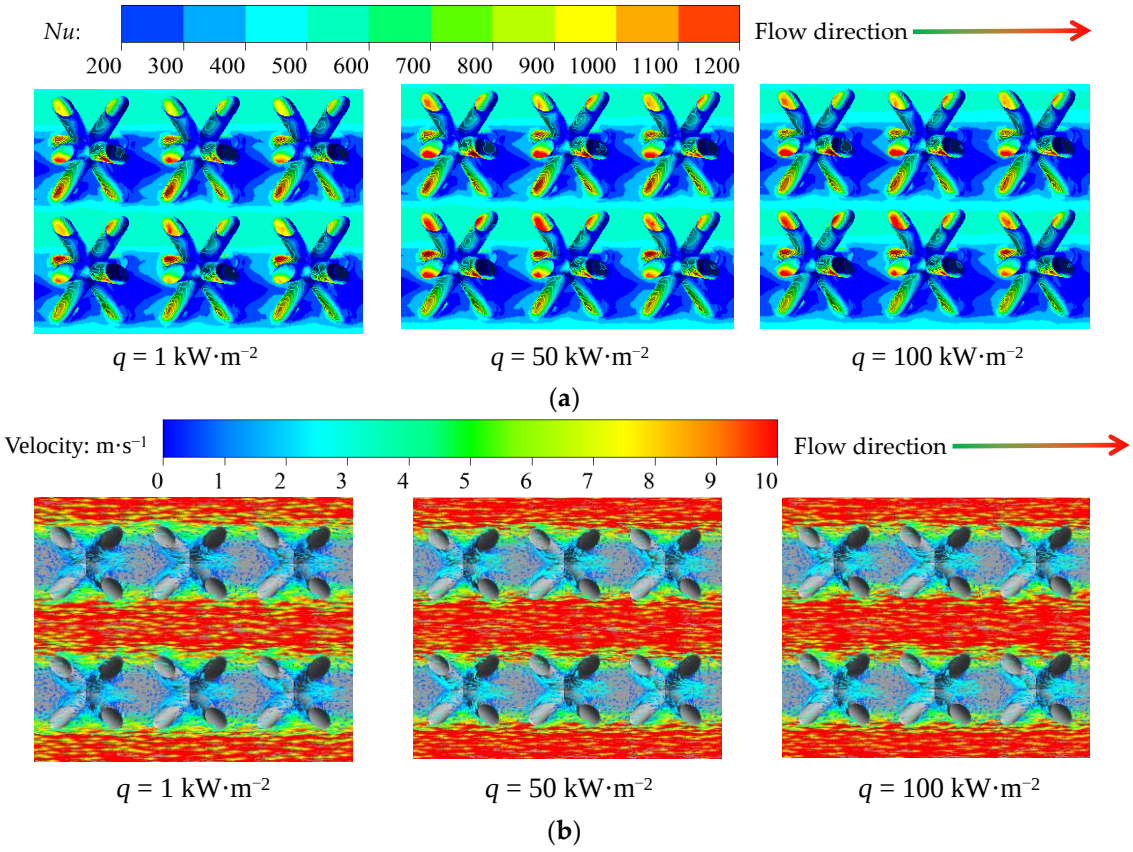

Figure 7. Distributions of heat transfer and flow field at various q under the actual operating conditions of gas turbine blades: (**a**) heat transfer distributions; (**b**) flow field distributions.

Figure 8 demonstrates the changing trends of the Nu_a, average Nusselt number ratio (Nu_a/Nu_0), f and F of the XTA channel with the q under the actual operating conditions (p_r = 2.5 MPa, T_r = 723 K) of gas turbine blades. As plotted in Figure 8a, with the increase in the q, the Nu_a of the XTA channel shows a trend of first rapidly increasing and then slightly decreasing or remaining unchanged, under different Re. This phenomenon shows that when the q is less than 10 kW·m^{-2}, the q has a significant influence on the heat transfer performance of the XTA channel. When the q is greater than 10 kW·m^{-2}, the change in the q hardly affects the heat transfer performance of the XTA channel. At different Re, compared with the lowest wall heat flux (q = 1 kW·m^{-2}), the Nu_a of the XTA channel at the highest wall heat flux (q = 100 kW·m^{-2}) is improved by about 2.84% to 32.09%. As plotted in Figure 8b, the changing trend of the Nu_a/Nu_0 of the XTA channel is the same as that of the Nu_a with the increase in the q at different Re. However, the Nu_a/Nu_0 of the XTA channel decrease with the increase in Re at different q. This is because the increase rate of the Nu_a with Re of the XTA channel is smaller relative to the smooth channel. This indicates that with the increase in Re, the heat transfer enhancement effect of the XTA channel relative to the smooth channel is weakened. As demonstrated in Figure 8c, with the increase in the q at different Re, the f of the XTA channel roughly shows a trend of first decreasing and then increasing. When compared with the lowest wall heat flux (q = 1 kW·m^{-2}) at various

Re, the *f* of the XTA channel at the highest wall heat flux (q = 100 kW·m^{-2}) is increased by about 0.73% to 1.89%. As shown in Figure 8d, similar to the variation trend of the Nu_a, the *F* of the XTA channel also shows a trend of first rapidly increasing and then slightly decreasing or remaining unchanged along with the increase in the q. The calculation results show that the *F* of the XTA channel at the highest wall heat flux (q = 100 kW·m^{-2}) is improved by about 2.21% to 31.74% compared to the lowest wall heat flux (q = 1 kW·m^{-2}).

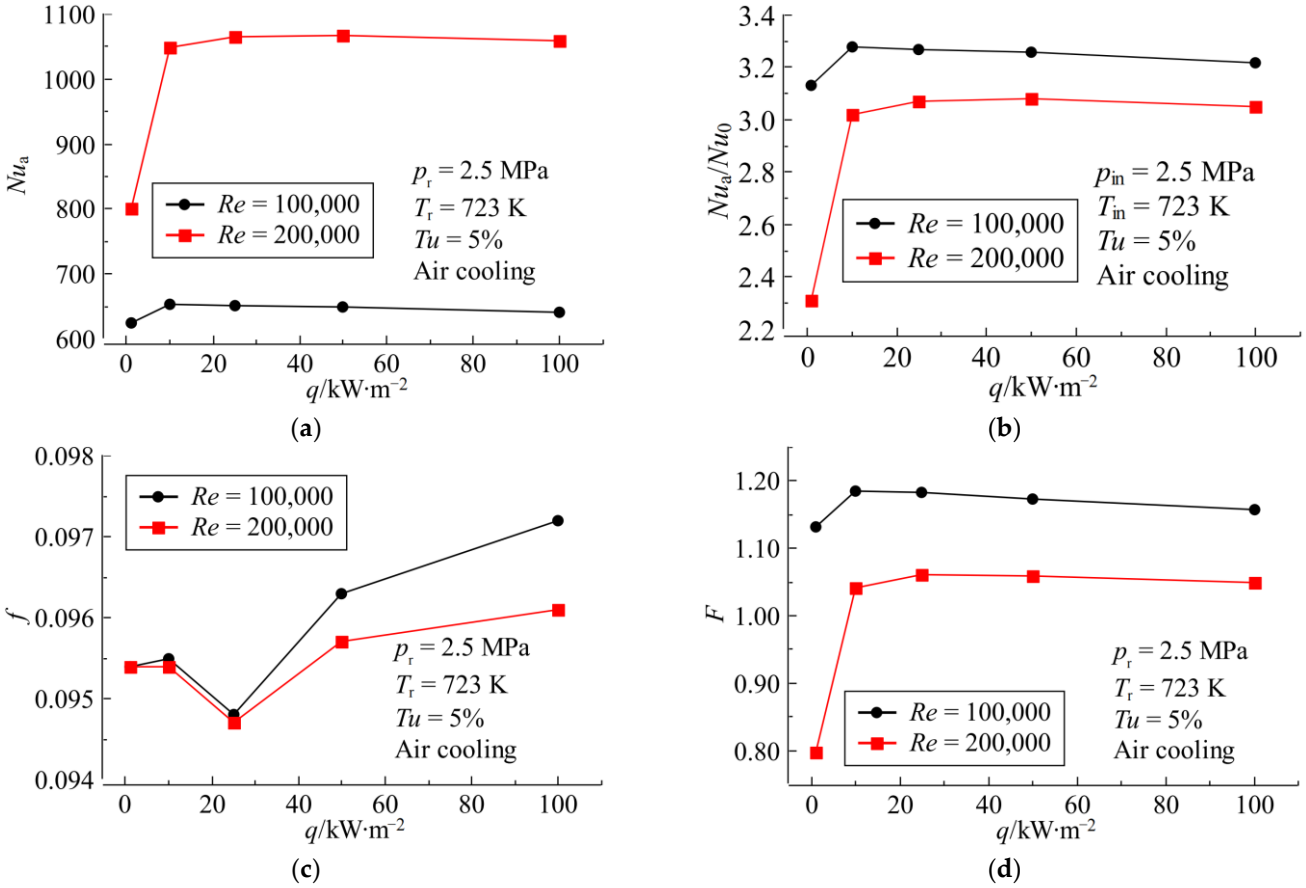

Figure 8. Effects of q on the cooling performance of XTA channel under actual operating conditions of gas turbine blades: (**a**,**b**) heat transfer performance; (**c**) flow performance; (**d**) comprehensive thermal performance.

4.4. Comparison of Air Cooling and Steam Cooling

The purpose of this section is to examine the application of steam-cooled XTA channel in gas turbine high-temperature blades. In the current gas turbine blades, the conventional cooling medium is the compressed air from the compressor. However, with the development of advanced gas turbines, air cooling is facing the problem of an insufficient cooling effect. Steam is considered a new cooling medium that can replace air because of its higher specific heat, and it has been applied in some G/H-class gas turbines of the gas–steam combined cycle unit. At present, several investigations have been conducted regarding the steam cooling of gas turbine blades and pointed out that the heat transfer performance of steam cooling is obviously better than that of air cooling [40]. Thus, it is essential to understand the flow and heat transfer characteristics of the steam-cooled XTA channels under the actual operating conditions of gas turbine blades and compare the performance differences between the steam-cooled XTA channels and the air-cooled XTA channels. The findings may provide some rules for the application of the steam-cooled XTA channels in the gas–steam combined cycle unit. It is worth mentioning that the physical parameters of the steam in the numerical solutions were derived from

IAPWS-IF97 material library in CFX-Pre, and a suitable steam model (i.e., Steam4 model) was selected according to the ranges of the studied operating conditions.

Figure 9 depicts the contour maps of *Nu* on the truss rod surface and channel wall and the plots of velocity vector in the channel for the air-cooled and steam-cooled XTA channels under the actual operating conditions (p_r = 2.5 MPa, T_r = 723 K) of the gas turbine high-temperature blades. Other operating conditions are as follows: *Re* = 100,000, *Tu* = 5%, q = 25 kW·m^{-2}. As depicted in Figure 9a, when compared with the air-cooled XTA channel, the *Nu* on both the truss rod surface and the channel wall of the steam-cooled XTA channel are visibly improved. Particularly, the local heat transfer improvement of the steam-cooled XTA channel is the most evident in the high heat transfer areas such as the channel wall between two rows of truss elements and the truss rod windward surfaces near the truss rod ends. Therefore, the use of steam cooling can effectively enhance the heat transfer performance of the XTA channel under the actual operating conditions of gas turbine blades. This also shows that steam is a promising working medium for the cooling of gas turbine blades. As depicted in Figure 9b, when compared with the air-cooled XTA channel, the sizes of vortexes in the steam-cooled XTA channel are basically unchanged, while the steam velocity between two columns of truss elements is increased to a certain extent. This is also one of the reasons that steam cooling can improve the heat transfer performance of the XTA channel under the actual operating conditions of gas turbine blades.

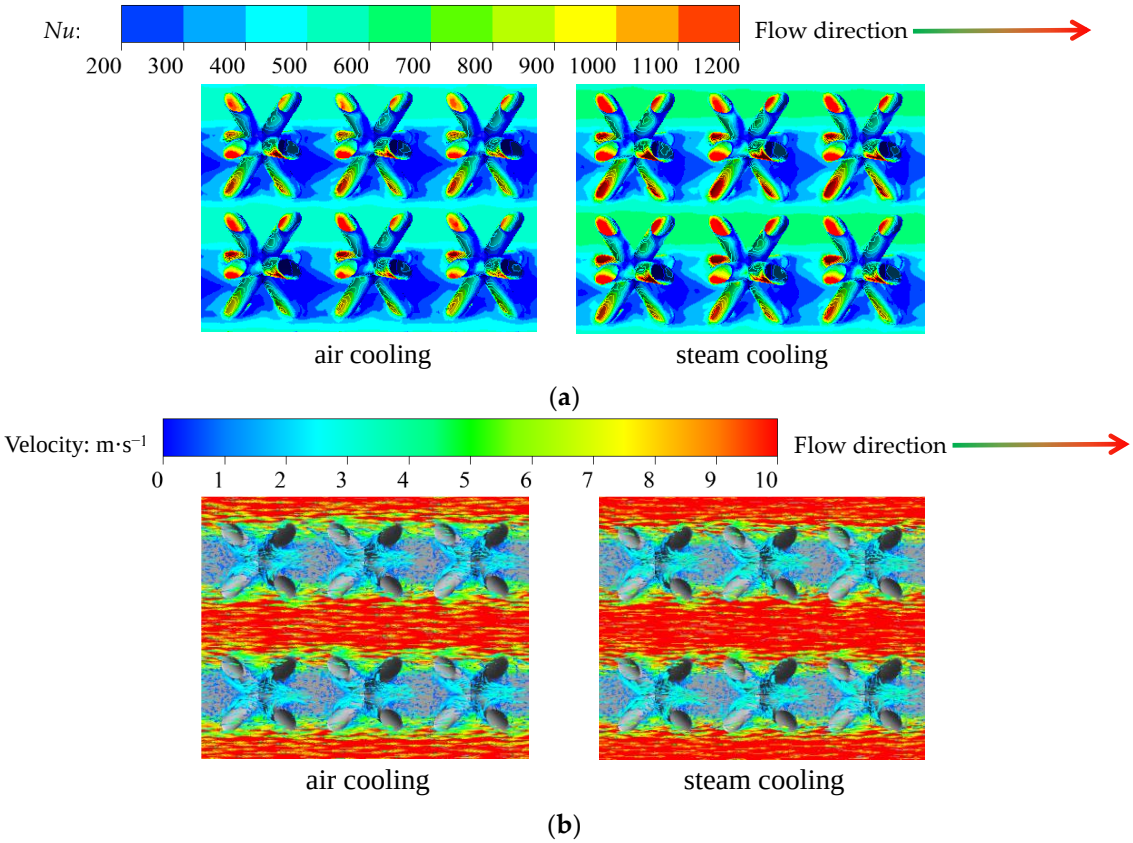

Figure 9. Comparison of distributions of heat transfer and flow field between the air-cooled XTA channel and the steam-cooled XTA channel under the actual operating conditions of gas turbine blades: (**a**) heat transfer distributions; (**b**) flow field distributions.

Figure 10 displays the comparison results of the Nu_a, f and F between the air-cooled XTA channel and the steam-cooled XTA channel under the actual operating conditions (p_r = 2.5 MPa, T_r = 723 K) of the gas turbine high-temperature blades. As shown in Figure 10a, under various *Re*, the heat transfer effect of the steam-cooled XTA channel is better than

that of the air-cooled XTA channel. Additionally, when the *Re* is high, the heat transfer enhancement advantage of the steam-cooled XTA channel is more obvious. This is because under the actual operating conditions (p_r = 2.5 MPa, T_r = 723 K) of the gas turbine high-temperature blades, the *Pr* of the cooling steam (Pr_{steam} = 0.939) is about 34.7% higher than the *Pr* of the cooling air (Pr_{air} = 0.697). Since the Nusselt number and *Pr* are positively related, i.e., $Nu_a \propto Pr^m$, where the value of *m* is generally 0.4. Thus, the heat transfer effect of the XTA channel under steam cooling is better than that under air cooling. The calculation results show that when the *Re* increases from 20,000 to 200,000, the Nu_a of the steam-cooled XTA channel is about 6.30% to 9.54% higher than that of the air-cooled XTA channel. As shown in Figure 10b, under various *Re*, the *f* of the steam-cooled XTA channel is slightly lower than that of the air-cooled XTA channel. When the *Re* varies from 20,000 to 200,000, the *f* of the steam-cooled XTA channel is reduced by 0.11% to 0.55% compared with that of the air-cooled XTA channel. As can be found from Figure 10c, the *F* of the steam-cooled XTA channel is lower than that of the air-cooled XTA channel at different *Re*. This is because although the Nu_a of the steam-cooled XTA channel is higher than that of the air-cooled XTA channel, the *Pr* of the steam is 34.7% higher than that of the air, so that the Nu_a of the steam-cooled smooth channel (i.e., Nu_0 in Equation (5)) is also much higher than that of the air-cooled smooth channel, as listed in Table 2. As a result, the values of Nu_a/Nu_0 of the steam-cooled XTA channel at different *Re* are obviously lower than that of the air-cooled XTA channel, while the differences in the corresponding values of f/f_0 between the steam-cooled XTA channel and the air-cooled XTA channel are very small, as shown in Table 2. Therefore, the calculation results of Equation (5) show that the *F* of the steam-cooled XTA channel is relatively lower. When the *Re* changes from 20,000 to 200,000, the *F* of the steam-cooled XTA channel is decreased by about 2.63% to 5.59% compared to that of the air-cooled XTA channel. In addition, it can also be seen from Figure 10 that for XTA channels with the same structural parameters, the varying laws of the Nu_a, *f* and *F* with the *Re* for steam cooling are basically the same as those for air cooling. This indicates that the flow and heat transfer characteristics, as well as the optimized structural parameters of the air-cooled XTA channels [39] previously reported by the authors of the present study, can be extended to the steam-cooled XTA channels.

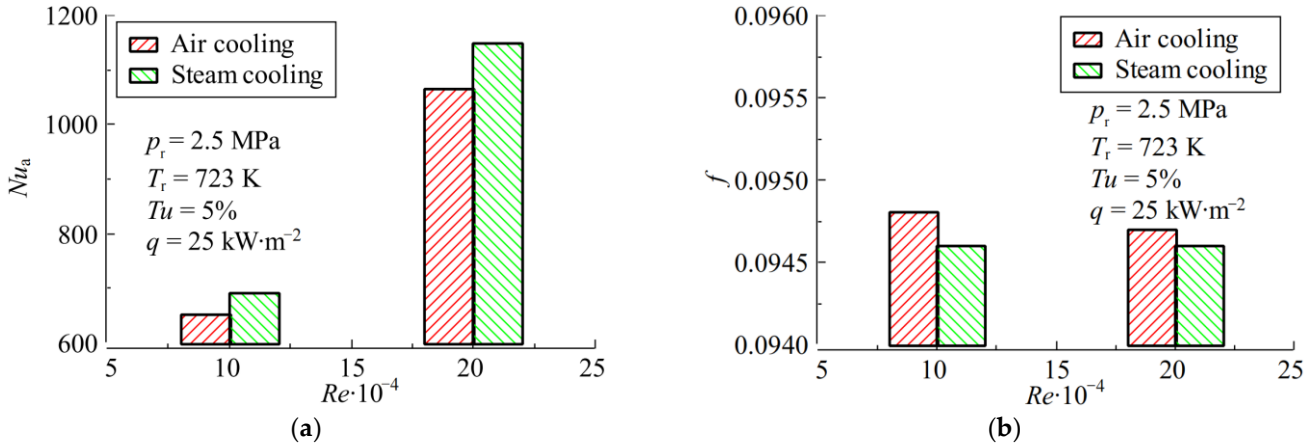

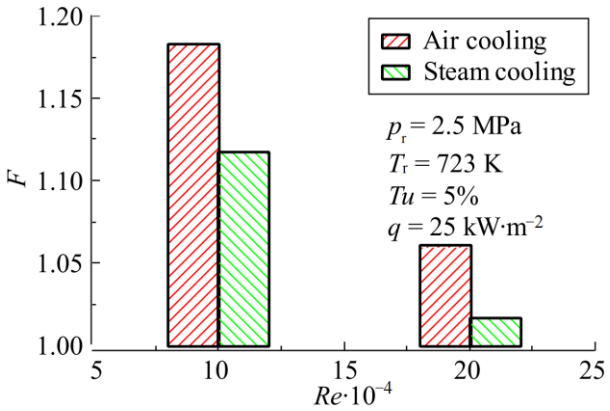

Figure 10. Comparison of the cooling performance between the air-cooled XTA channel and the steam-cooled XTA channel under the actual operating conditions of gas turbine blades: (**a**) heat transfer performance; (**b**) flow performance; (**c**) comprehensive thermal performance.

Table 2. Comparison of the Nu_a/Nu_0 and f/f_0 between the air-cooled XTA channel and the steam-cooled XTA channel.

	Air Cooling				**Steam Cooling**			
Re	Nu_0	f_0	Nu_a/Nu_0	f/f_0	Nu_0	f_0	Nu_a/Nu_0	f/f_0
100,000	199.08	0.0045	3.27	21.08	224.33	0.0045	3.08	21.03
200,000	346.61	0.0039	3.07	24.26	390.58	0.0039	2.94	24.23

4.5. Empirical Correlations

In order to increase the practicability of the research results of this work, the empirical correlations of Nu_a and f were fitted for the XTA channel under the actual operating conditions of the gas turbine high-temperature blades. In this investigation, the relationships between the Nu_a or f and Re, inlet Tu, q and Pr were assumed to be the widely used and convenient power functions [39]. The form of the assumed empirical correlation is as follows:

$$f(x) = aRe^bTu^c(q/q_{max})^dPr^e \quad (8)$$

where $f(x)$ is Nu_a or f; a, b, and c are the parameters to be fitted; q_{max} = 100,000 W·m^{-2} is the maximum wall heat flux studied in this study.

Based on the data obtained from numerical simulations in Sections 4.1 to 4.4 and through self-programming via Python language, the empirical correlations reflecting the influence laws of the Re, Tu, q and Pr on the Nu_a and f of the XTA channel under the actual operating conditions of gas turbine blades were fitted as follows:

$$Nu_a = 0.290Re^{0.688}Tu^{0.017}(q/q_{max})^{0.044}Pr^{0.248} \quad (9)$$

$$f = 0.171Re^{-0.047}Tu^{0.0086}(q/q_{max})^{0.0024}Pr^{-0.028} \quad (10)$$

The ranges of input parameters of Equations (9) and (10) are: 20,000 ≤ Re ≤ 200,000, 1% ≤ Tu ≤ 20%, 1000 W·m^{-2} ≤ q ≤ 100,000 W·m^{-2}, 0.697 ≤ Pr ≤ 0.939.

The distribution curves of fitting deviations for Equations (9) and (10) are displayed in Figure 11. As shown, the maximum fitting deviations of the heat transfer correlation and friction correlation for the XTA channel under various actual operating conditions of gas turbine blades are 13.84% and −3.60%, respectively. The mean fitting deviations of the heat transfer correlation and friction correlation are 2.53% and 1.65%, respectively. Consequently, the above fitted empirical correlations can comparatively accurately evaluate the heat transfer performance, flow performance and comprehensive thermal

performance of the XTA channel under the actual operating conditions of the gas turbine high-temperature blades.

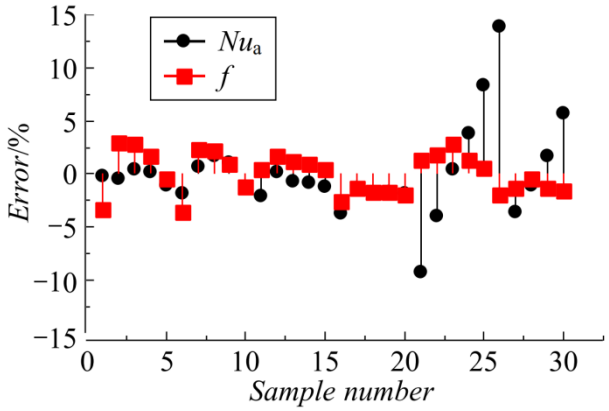

Figure 11. Fitting deviations.

5. Conclusions

In this study, the heat transfer and fluid flow capabilities of an XTA cooling channel under different operating conditions of gas turbine blades were thoroughly studied. The main conclusions are as follows:

(1) Among the three parameters of inlet *Re*, inlet *Tu* and *q*, the inlet *Re* has the most significant effect on the flow and heat transfer performance of the XTA channel.
(2) When the inlet *Re* increases from 20,000 to 200,000, the Nu_a of the XTA channel is increased by 3.92 times, the *f* is decreased by 12.88% and the *F* is decreased by 31.19%.
(3) Compared with the medium turbulence intensity (*Tu* = 5%), the Nu_a, *f* and *F* of the XTA channel at *Tu* = 20% are increased by 3.70%, 2.51% and 2.79%, respectively.
(4) With the increase in the *q*, the *f* of the XTA channel roughly shows a trend of first decreasing and then increasing, while the Nu_a and the *F* show a trend of first rapidly increasing and then slightly decreasing or remaining unchanged.
(5) Compared with air cooling, the Nu_a of the XTA channel of steam cooling are increased by 6.30% to 9.54%, and the corresponding *f* and *F* are decreased by 0.11% to 0.55% and 2.63% to 5.59%, respectively.
(6) The empirical correlations of Nu_a and *f* for the XTA cooling channel under different operating conditions were fitted; the corresponding maximum fitting deviations are within ± 14%.

Author Contributions: Conceptualization, L.X. (Lei Xi). and J.G.; methodology, L.X. (Lei Xi); validation, L.X. (Lei Xi), J.G., and L.X. (Liang Xu); formal analysis, T.Y.; investigation, Z.Z.; resources, J.G.; data curation, Z.Z.; writing—original draft preparation, L.X. (Lei Xi); writing—review and editing, Z.Z.; visualization, T.Y.; supervision, Y.L. and L.X. (Lei Xi); project administration, Y.L. and J.G. All authors have read and agreed to the published version of the manuscript.

Funding: The authors would like to express their sincere gratitude to the Project Supported by Natural Science Basic Research Plan in Shaanxi Province of China (2022JQ-545), the Project funded by China Postdoctoral Science Foundation (2021M702573) and the National Natural Science Foundation of China (51876157) for providing financial support for this work.

Data Availability Statement: Not applicable.

Conflicts of Interest: The authors declare no conflicts of interest.

Nomenclature

C	Characteristic length of the truss element, mm.
D	Diameter of the truss rod, mm.
F	Friction coefficient of the XTA channel.
f_0	Friction coefficient of the smooth channel.
F	Comprehensive thermal coefficient.
H	Height of the subchannel near the wall, mm.
H	Height of the channel, mm.
L	Length of the channel, mm.
Nu	Local Nusselt number of the XTA channel.
Nu_a	Average Nusselt number of the XTA channel.
Nu_0	Average Nusselt number of the smooth channel.
p_r	Reference pressure of the cooling medium, Pa.
Pr	Prandtl number.
q	Local wall heat flux, $W \cdot m^{-2}$.
Q_{max}	Maximum heat flux in this study, $W \cdot m^{-2}$.
Re	Inlet Reynolds number.
T_c	Local bulk fluid temperature, K.
T_r	Reference temperature of the cooling medium, Pa.
T_w	Local wall temperature, K.
Tu	Inlet turbulence intensity, %.
U	Inlet velocity of the cooling medium, $m \cdot s^{-1}$.
W	Width of the channel, mm.
X_s	Transverse spacing of adjacent truss elements, mm.
Z_s	Streamwise spacing of adjacent truss elements, mm.
Greek symbols	
β	Truss rod inclination angle, °.
δ	Wall thickness of the channel, mm.
Δp	Pressure drop across the channel, Pa.
λ	Heat conductivity of the cooling medium, $W \cdot m^{-1} \cdot K^{-1}$.
ρ	Density of the cooling medium, $kg \cdot m^{-3}$.
Υ	Kinematic viscosity of the cooling medium, $m^2 \cdot s^{-1}$.

References

1. Wang, Q.; Yang, L.; Huang, K. Fast prediction and sensitivity analysis of gas turbine cooling performance using supervised learning approaches. *Energy* **2022**, *246*, 123373. https://doi.org/10.1016/j.energy.2022.123373.
2. Xi, L.; Gao, J.; Xu, L.; Zhao, Z.; Ruan, Q.; Li, Y. Numerical investigation and parameter sensitivity analysis on flow and heat transfer performance of jet array impingement cooling in a quasi-leading-edge channel. *Aerospace* **2022**, *9*, 87. https://doi.org/10.3390/aerospace9020087.
3. Anwajler, B. The thermal properties of a prototype insulation with a gyroid structure—optimization of the structure of a cellular composite made using SLS printing technology. *Materials* **2022**, *15*, 1352. https://doi.org/10.3390/ma15041352.
4. Li, S.; Jiang, W.; Zhu, X.; Xie, X. Effect of localized defects on mechanical and creep properties for pyramidal lattice truss panel structure by analytical, experimental and finite element methods. *Thin Wall. Struct.* **2022**, *170*, 108531. https://doi.org/10.1016/j.tws.2021.108531.
5. Park, K.-M.; Min, K.-S.; Roh, Y.-S. Design optimization of lattice structures under compression: Study of unit cell types and cell arrangements. *Materials* **2022**, *15*, 97. https://doi.org/10.3390/ma15010097.
6. Ho, J.Y.; Leong, K.C.; Wong, T.N. Experimental and numerical investigation of forced convection heat transfer in porous lattice structures produced by selective laser melting. *Int. J. Therm. Sci.* **2019**, *137*, 276–287. https://doi.org/10.1016/j.ijthermalsci.2018.11.022.
7. Ho, J.Y.; Leong, K.C.; Wong, T.N. Additively-manufactured metallic porous lattice heat exchangers for air-side heat transfer enhancement. *Int. J. Heat Mass Transf.* **2020**, *150*, 119262. https://doi.org/10.1016/j.ijheatmasstransfer.2019.119262.
8. Chen, Y.; Nassar, H.; Huang, G. Discrete transformation elasticity: An approach to design lattice-based polar metamaterials. *Int. J. Eng. Sci.* **2021**, *168*, 103562. https://doi.org/10.1016/j.ijengsci.2021.103562.
9. Zhang, Q.; Han, Y.; Chen, C.; Lu, T. Ultralight X-type lattice sandwich structure (I): Concept, fabrication and experimental characterization. *Sci. China Ser. E* **2009**, *52*, 2147–2154. https://doi.org/10.1007/s11431-009-0219-9.

10. Al-Ketan, O.; Lee, D.W.; Rowshan, R.; Al-Rub, R.K.A. Functionally graded and multi-morphology sheet TPMS lattices: Design, manufacturing, and mechanical properties. *J. Mech. Behav. Biomed.* **2020**, *102*, 103520. https://doi.org/10.1016/j.jmbbm.2019.103520.
11. Plessis, A.D.; Razavi, S.M.J.; Benedetti, M.; Murchio, S.; Leary, M.; Watson, M.; Berto, F. Properties and applications of additively manufactured metallic cellular materials: A review. *Prog. Mater. Sci.* **2021**, *125*, 100918. https://doi.org/10.1016/j.pmatsci.2021.100918.
12. Kladovasilakis, N.; Charalampous, P.; Tsongas, K.; Kostavelis, I.; Tzetzis, D.; Tzovaras, D. Experimental and computational investigation of lattice sandwich structures constructed by additive manufacturing technologies. *J. Manuf. Mater. Process.* **2021**, *5*, 95. https://doi.org/10.3390/jmmp5030095.
13. Joo, J.H.; Kang, K.J.; Kim, T.; Lu, T.J. Forced convective heat transfer in all metallic wire-woven bulk Kagome sandwich panels. *Int. J. Heat Mass Transf.* **2011**, *54*, 5658–5662. https://doi.org/10.1016/j.ijheatmasstransfer.2011.08.018.
14. Ullah, I.; Elambasseril, J.; Brandt, M.; Feih, S. Performance of bio-inspired Kagome truss core structures under compression and shear loading. *Compos. Struct*. **2014**, *118*, 294–302. https://doi.org/10.1016/j.compstruct.2014.07.036.
15. Yan, H.B.; Zhang, Q.C.; Lu, T.J. Heat transfer enhancement by X-type lattice in ventilated brake disc. *Int. J. Therm. Sci.* **2016**, *107*, 39–55. https://doi.org/10.1016/j.ijthermalsci.2016.03.026.
16. Akzhigitov, D.; Srymbetov, T.; Aldabergen, A.; Spitas, C. Structural and Aerodynamical Parametric Study of Truss-Core Gas Turbine Rotor Blade. *J. Appl. Comput. Mech.* **2021**, *7*, 831–838, https://doi.org/10.22055/jacm.2020.35467.2667.
17. Yang, G.; Hou, C.; Zhao, M.; Mao, W. Comparison of convective heat transfer for kagome and tetrahedral truss-cored lattice sandwich panels. *Sci. Rep*. **2019**, *9*, 3731. https://doi.org/10.1038/s41598-019-39704-2.
18. Kemerli, U.; Kahveci, K. Conjugate forced convective heat transfer in a sandwich panel with a kagome truss core: The effects of strut length and diameter. *Appl. Therm. Eng.* **2020**, *167*, 114794. https://doi.org/10.1016/j.applthermaleng.2019.114794.
19. Ma, Y.; Yan, H.; Hooman, K.; Xie, G. Enhanced heat transfer in a pyramidal lattice sandwich panel by introducing pin-fins/protrusions/dimples. *Int. J. Therm. Sci.* **2020**, *156*, 106468. https://doi.org/10.1016/j.ijthermalsci.2020.106468.
20. Deb, D.; Rajan, H.; Kundu, R.; Mohan, R. CFD and machine learning based simulation of flow and heat transfer characteristics of micro lattice structures. *IOP Conf. Ser. Earth Environ. Sci.* **2021**, *850*, 012034. https://doi.org/10.1088/1755-1315/850/1/012034.
21. Lai, X.; Wang, C.; Peng, D.; Yang, H.; Wei, Z. Analysis of heat transfer characteristics of a heat exchanger based on a lattice filling. *Coatings* **2021**, *11*, 1089. https://doi.org/10.3390/coatings11091089.
22. Righetti, G.; Longo, G.A.; Mancin, S.; Zilio, C. Shape optimization of lattice-frame materials obtained via additive manufacturing during air forced convection. *Exp. Heat Transfer* **2022**, *35*, 1–16. https://doi.org/10.1080/08916152.2022.2084472.
23. Caket, A.G.; Wang, C.; Nugroho, M.A.; Celik, H.; Mobedi, M. Recent studies on 3D lattice metal frame technique for enhancement of heat transfer: Discovering trends and reasons. *Renew. Sust. Energ. Rev.* **2022**, *167*, 112697. https://doi.org/10.1016/j.rser.2022.112697.
24. Bai, X.; Liu, C.; Zhang, C.; Meng, X.; Li, J.; Zhang, X. A comprehensive study on the heat transfer characteristics of windward bend lattice frame structure. *Propuls. Power Res.* **2022**, *11*, 1–15. https://doi.org/10.1016/j.jppr.2022.03.003.
25. Aider, Y.; Kaur, I.; Cho, H.; Singh, P. Periodic heat transfer characteristics of additively manufactured lattices. *Int. J. Heat Mass Transf.* **2022**, *189*, 122692. https://doi.org/10.1016/j.ijheatmasstransfer.2022.122692.
26. Shahrzadi, M.; Emami, M.D.; Akbarzadeh, A.H. Heat transfer in BCC lattice materials: Conduction, convection, and radiation. *Compos. Struct.* **2022**, *284*, 115159. https://doi.org/10.1016/j.compstruct.2021.115159.
27. Kaur, I.; Singh, P. Conjugate heat transfer in lattice frame materials based on novel unit cell topologies. *Numer. Heat Tr. A-Appl.* **2022**, *82*, 1–14. https://doi.org/10.1080/10407782.2022.2083874.
28. Kaur, I.; Singh, P. Direct pore-scale simulations of fully periodic unit cells of different regular lattices. *J. Heat Trans-T. ASME* **2022**, *144*, 022702. https://doi.org/10.1115/1.4053204.
29. Alkebsi, E.A.A.; Ameddah, H.; Outtas, T.; Almutawakel, A. Design of graded lattice structures in turbine blades using topology optimization. *Int. J. Comput. Integ. M.* **2021**, *34*, 370–384. https://doi.org/10.1080/0951192X.2021.1872106.
30. Hussain, S.; Ghopa, W.A.W.; Singh, S.S.K.; Azman, A.H.; Abdullah, S. Experimental and numerical vibration analysis of octet-truss-lattice-based gas turbine blades. *Metals* **2022**, *12*, 340. https://doi.org/10.3390/met12020340.
31. Shen, B.; Li, Y.; Yan, H.; Boetcher, S.K.; Xie, G. Heat transfer enhancement of wedge-shaped channels by replacing pin fins with kagome lattice structures. *Int. J. Heat Mass Transf.* **2019**, *141*, 88–101. https://doi.org/10.1016/j.ijheatmasstransfer.2019.06.059.
32. Xu, L.; Ruan, Q.; Shen, Q.; Xi, L.; Gao, J.; Li, Y. Optimization design of lattice structures in internal cooling channel with variable aspect ratio of gas turbine blade. *Energies* **2021**, *14*, 3954. https://doi.org/10.3390/en14133954.
33. Xu, L.; Shen, Q.; Ruan, Q.; Xi, L.; Gao, J.; Li, Y. Optimization design of lattice structures in internal cooling channel of turbine blade. *Appl. Sci.* **2021**, *11*, 5838. https://doi.org/10.3390/app11135838.
34. Kaur, I.; Aider, Y.; Nithyanandam, K.; Singh, P. Thermal-hydraulic performance of additively manufactured lattices for gas turbine blade trailing edge cooling. *Appl. Therm. Eng.* **2022**, *211*, 118461. https://doi.org/10.1016/j.applthermaleng.2022.118461.
35. Liang, D.; He, G.; Chen, W.; Chen, Y.; Chyu, M.K. Fluid flow and heat transfer performance for micro-lattice structures fabricated by Selective Laser Melting. *Int. J. Therm. Sci.* **2022**, *172*, 107312.
36. Fu, Q.; Luo, X.; Chen, W.; Chyu, M.K. Numerical investigation of the effects of lattice array structures on film cooling performance. *Energies* **2022**, *15*, 4711. https://doi.org/10.3390/en15134711.
37. Xi, L.; Xu, L.; Gao, J.; Zhao, Z.; Li, Y. Study on flow and heat transfer performance of X-type truss array cooling channel. *Case Stud. Therm. Eng.* **2021**, *26*, 101034. https://doi.org/10.1016/j.csite.2021.101034.

38. Xi, L.; Xu, L.; Gao, J.; Zhao, Z.; Li, Y. Cooling performance analysis and structural parameter optimization of X-shaped truss array channel based on neural networks and genetic algorithm. *Int. J. Heat Mass Transf.* **2022**, *186*, 122452. https://doi.org/10.1016/j.ijheatmasstransfer.2021.122452.
39. Xi, L.; Gao, J.; Xu, L.; Zhao, Z.; Yang, Z.; Li, Y. Numerical investigation on cooling performance of rectangular channels filled with X-shaped truss array structures. *Aerospace* **2022**, *9*, 405. https://doi.org/10.3390/aerospace9080405.
40. Xu, L.; Wang, W.; Gao, T.; Shi, X.; Gao, J.; Liang, W. Experimental study on cooling performance of a steam-cooled turbine blade with five internal cooling smooth channels. *Exp. Therm. Fluid Sci.* **2014**, *58*, 180–187. https://doi.org/10.1016/j.expthermflusci.2014.07.004.